Characterization of Microstrip Lines near a Substrate Edge and Design Formulas of Edge-Compensated Microstrip Lines

EIKICHI YAMASHITA, FELLOW, IEEE, HIDEYUKI OHASHI, AND KAZUHIKO ATSUKI

Abstract — **The proximity effects of microstrip lines near a substrate edge have been pointed out by Pucel as a problem for effectively designing high-packing-density MMIC's. Proximity effects of this type are analyzed by using the rectangular boundary division method. The concept of edge-compensated microstrip lines (ECM lines) is introduced, whereby we can circumvent the proximity effects on the characteristic impedance. The design parameters of the ECM lines are given in the form of simple polynomials together with numerical data. Some experimental results on the line capacitance agree with the theory, with errors of about 1 percent.**

I. INTRODUCTION

MICROSTRIP (MS) lines have been employed as interconnections between elements in monolithic microwave integrated circuits (MMIC's), which hold promise for many new microwave device applications. Pucel has pointed out the significance of "proximity effects" of two types which appear when designing circuit patterns of high-packing-density GaAs MMIC's and calls attention to the absence of analysis methods to estimate the effects theoretically [1], [2].

One type of proximity effect is observed when a strip conductor is near a conductor having ground potential on the top surface of the substrate. This type has already been analyzed by one of the authors in a recent paper [3]. The second type is observed when a strip conductor is located close to a substrate edge. Estimation methods or exact CAD methods for these proximity effects are urgently required to avoid tweaking after fabrication processes. The characteristics of the finite-width open microstrip line have been studied based on a free-space Green's function approach in the past [4].

In this paper, the proximity effects of the second type are analyzed by using the rectangular boundary division method proposed in a previous paper [5]. It is assumed that the cross-sectional dimensions of transmission lines in MMIC's are small compared with the wavelengths. This validates the use of the quasi-TEM wave approximation.

Manuscript received September 6, 1988; revised December 8, 1988. This work was supported in part by a grant-in-aid from the Ministry of Education, Science and Culture, Japan.

E. Yamashita and K. Atsuki are with the University of Electro-communications, Chofu-shi, Tokyo, 182 Japan.

H. Ohashi was with the University of Electro-communications, Chofu-shi, Tokyo, Japan. He is now with the Information Systems and Electronics Development Laboratory, Mitsubishi Electric Corporation, Kamakura, Japan.

IEEE Log Number 8926577.

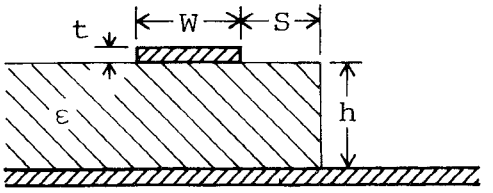

Fig. 1. Microstrip lines with a substrate edge (also the structure of edge-compensated microstrip lines, defined in Section IV).

Then, the concept of edge-compensated microstrip lines to keep the characteristic impedance constant near a substrate edge is introduced to circumvent the proximity effects and to expand the interconnection flexibility of microstrip lines on MMIC substrates. The practical design parameters of the edge-compensated microstrip lines are given in the form of numerical data and simple polynomials for CAD work with a curve-fitting procedure. Results of capacitance measurements are compared with this theory.

II. RECTANGULAR BOUNDARY DIVISION METHOD FOR ESTIMATING SUBSTRATE EDGE EFFECTS

Fig. 1 shows the structure to be treated here. When the microstrip conductor on the top of the substrate is located close to an edge of the substrate and the dimension of the separation S is decreased, the capacitance between the strip and the ground conductor is also decreased. Consequently, the characteristic impedance is increased. Therefore, if this proximity effect is to be circumvented in high-packing-density MMIC's, tolerable sizes for S should be determined before fabrication. The rectangular boundary division method, which has been discussed in a previous paper for treating the proximity effects of the first type, is employed here because each dielectric region in this structure is of the rectangular shape suited to this method, as shown in Fig. 2. The substrate thickness h and the strip width W are assumed to be sufficiently small compared with wavelengths in order to validate the use of the quasi-TEM wave approximation. The thickness of the strip conductor t is assumed to be negligible in this paper.

Scalar potentials as the solutions of Laplace's equation are first expanded in Fourier series in each rectangular

0018-9480/89/0500-0890$01.00

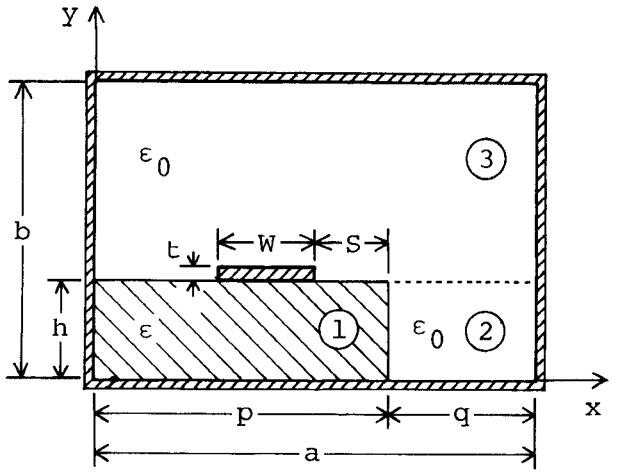

Fig. 2. Total structure under study with relevant subareas.

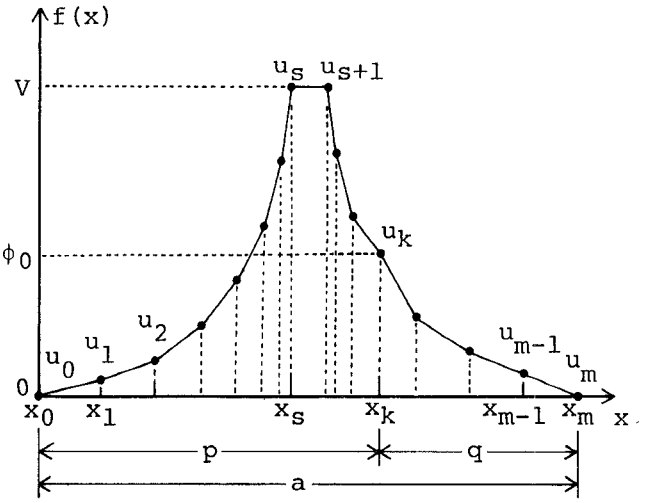

Fig. 3. Spline-knot potential distribution.

region as follows:

$$\phi_1(x,y)=\phi_{10}(x,y)+\sum_{n=1}^{\infty}A_n\sinh(\xi_{1n}y)\sin(\xi_{1n}x)$$
$$\text{(region 1; } 0\leqslant x\leqslant p,\ 0\leqslant y\leqslant h\text{)} \tag{1a}$$

$$\phi_2(x,y)=\phi_{20}(x,y)+\sum_{n=1}^{\infty}B_n\sinh(\xi_{2n}y)\sin(\xi_{2n}(a-x))$$
$$\text{(region 2; } p\leqslant x\leqslant a,\ 0\leqslant y\leqslant h\text{)} \tag{1b}$$

$$\phi_3(x,y)=\sum_{n=1}^{\infty}C_n\sinh(\xi_{3n}(b-y))\sin(\xi_{3n}x)$$
$$\text{(region 3; } 0\leqslant x\leqslant a,\ h\leqslant y\leqslant b\text{)} \tag{1c}$$

where

$$\xi_{1n}=\frac{n\pi}{p}\qquad \xi_{2n}=\frac{n\pi}{q}\qquad \xi_{3n}=\frac{n\pi}{a} \tag{1d}$$

and A_n, B_n, and C_n are unknown coefficients.

Each term of the Fourier series given in (1a) and (1b) vanishes at the boundary between regions 1 and 2, as well as at conductor walls. Two functions, $\phi_{10}(x,y)$ and $\phi_{20}(x,y)$, have been added in the above expressions to give the potential on the boundary line ($x=p$, $0\leqslant y\leqslant h$).

Since $\phi_{10}(x,y)$ and $\phi_{20}(x,y)$ should also satisfy Laplace's equation, we take approximate forms for these functions as

$$\phi_{10}(x,y)=\frac{xy}{ph}\phi_0 \tag{2a}$$

$$\phi_{20}(x,y)=\frac{(a-x)y}{qh}\phi_0 \tag{2b}$$

where ϕ_0 is defined as the potential at the dielectric corner point, $x=p$, $y=h$.

The total electric field energy for these potential functions is given by

$$U=\sum_{\nu=1}^{3}\frac{1}{2}\epsilon_\nu\iint_{S_\nu}\left[\left(\frac{\partial\phi_\nu}{\partial x}\right)^2+\left(\frac{\partial\phi_\nu}{\partial y}\right)^2\right]dx\,dy \tag{3}$$

where ϵ_ν and S_ν denote the dielectric permittivity and the cross-sectional area of the region ν ($\nu=1,2,3$). It is known in electrostatics that exact potential functions should minimize the total energy U. Instead of minimizing U by selecting an infinite number of unknown coefficients, A_n, B_n, and C_n, we use a finite number of spline-knot potentials which represent potentials on the boundary line defined by $y=h$. That is, the potential on the boundary, $f(x)$, is approximately described with the first-order spline function as

$$f(x)=\sum_{i=1}^{m}F_i(x)\qquad (0\leqslant x\leqslant a,\ y=h) \tag{4a}$$

where

$$F_i(x)=\begin{cases}\dfrac{u_i(x-x_{i-1})+u_{i-1}(x_i-x)}{x_i-x_{i-1}} & (x_{i-1}\leqslant x\leqslant x_i)\\ 0 & \text{(otherwise).}\end{cases} \tag{4b}$$

Fig. 3 shows how the spline-knot potentials are distributed on the boundary line, $y=h$. Because the potential at the strip conductor is given by V, $u_s=u_{s+1}=V$ and $u_0=u_m=0$. We also note that ϕ_0 is equal to u_k. Substituting (4) into (1), we can express the Fourier coefficients in terms of the spline-knot potentials $u_i(i=1,2,\cdots,m-1)$ as

$$A_n=\frac{2\sum_{i=1}^{k}A_{ni}u_i}{p\sinh(\xi_{1n}h)} \tag{5a}$$

$$B_n=\frac{2\sum_{i=k}^{m-1}B_{ni}u_i}{q\sinh(\xi_{2n}h)} \tag{5b}$$

$$C_n = \frac{2\sum_{i=1}^{m-1} C_{ni} u_i}{a \sinh(\xi_{3n}(b-h))} \tag{5c}$$

where A_{ni}, B_{ni}, and C_{ni} are defined in Appendix I.

Having found the coefficients, A_n, B_n, and C_n, in terms of spline-knot potentials u_i $(i=1,2,\cdots,m-1)$, we can carry out the total energy integration (3). The result of the integration is written in the following form:

$$U = \sum_{i=1}^{m-1}\sum_{j=1}^{m-1} \alpha_{ij} u_i u_j \tag{6}$$

where α_{ij} $(i,\ j=1,2,\cdots,m-1)$ are given in Appendix II.

When we impose the minimum energy condition on the spline-knot potentials as

$$\frac{\partial U}{\partial u_i} = 0 \qquad (i=1,2,\cdots,m-1) \tag{7}$$

we obtain a set of linear equations for the spline-knot variables u_i. Since part of these variables are given as the strip conductor potential $u_s = u_{s+1} = V$, these equations become inhomogeneous, as shown below, and can be solved on a computer:

$$\sum_{\substack{j=1 \\ j\neq s,s+1}}^{m-1} \alpha_{ij} u_j = -(\alpha_{is} + \alpha_{is+1})V$$

$$(i=1,2,\cdots,s-1,\ s+2,\cdots,m-1). \tag{8}$$

Substituting the solutions of the spline-knot potentials into the expressions of the Fourier coefficients and then into those of the total energy, we obtain the line capacitance as

$$C = \frac{2U}{V^2}. \tag{9}$$

In similar fashion, when the dielectric materials in the structure are replaced by air, the line capacitance is given by the corresponding total energy U_0 as

$$C_0 = \frac{2U_0}{V^2}. \tag{10}$$

The characteristic impedance Z, the effective dielectric constant ϵ_{eff}, and the wavelength reduction factor λ/λ_0 can be obtained, respectively, by

$$Z = \frac{1}{v_0\sqrt{CC_0}} \tag{11}$$

$$\epsilon_{\text{eff}} = \frac{C}{C_0} \tag{12}$$

and

$$\frac{\lambda}{\lambda_0} = \frac{1}{\sqrt{\epsilon_{\text{eff}}}} \tag{13}$$

where v_0 is the light velocity in vacuum.

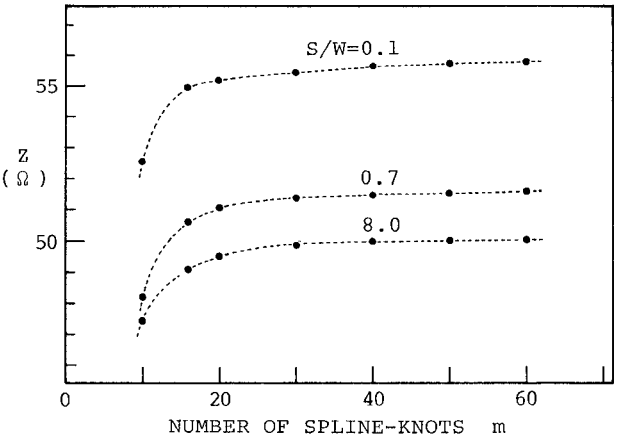

Fig. 4. Numerical convergence property of the characteristic impedance against the number of spline-knots. $h/W=1.382$, $a/W=b/W=27.6$, $a/2=q+S+W/2$, $\epsilon_r=12.9$, $N=2000$.

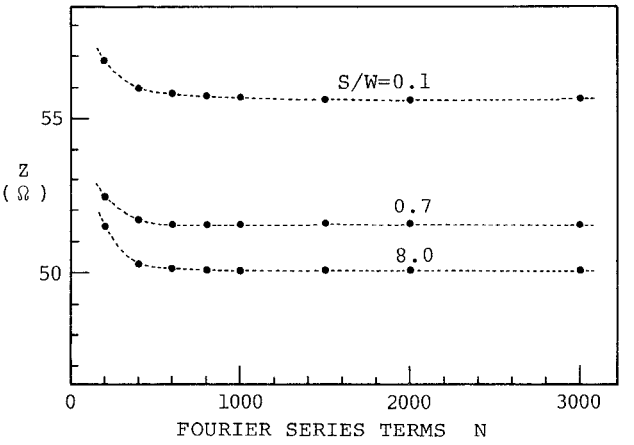

Fig. 5 Numerical convergence property of the characteristic impedance against the number of Fourier series terms. $h/W=1.382$, $a/W=b/W=27.6$, $a/2=q+S+W/2$, $\epsilon_r=12.9$, $m=60$.

III. Numerical and Experimental Results

Figs. 4 and 5 show the numerical convergence properties of the characteristic impedance against the number of spline-knots m and the Fourier series terms N, respectively. These results indicate that satisfactory numbers for the convergence are given by $m \geqslant 50$ and $N \geqslant 2000$. The computation time needed for the characterization of one structure is about 6 s on the HITAC M260H computer.

Figs. 6 and 7 show the estimated proximity effects on the characteristic impedance and on the wavelength reduction factor, respectively, for the case of GaAs substrate ($\epsilon_r=12.9$) and alumina ceramic substrate ($\epsilon_r=9.7$). The numerical results given above were obtained by locating strip conductors at the center of substrates (i.e., $a/2=q+S+W/2$) and giving sufficiently large values for the separation between strip conductors and outer conductor walls (i.e., $a/W=b/W=27.6$) to eliminate the effect of the outer conductor. Figs. 8 and 9 show the proximity effects of a vertical conductor wall near the substrate edge on the characteristic impedance and on the wavelength reduction factor, respectively, for the case of GaAs substrate.

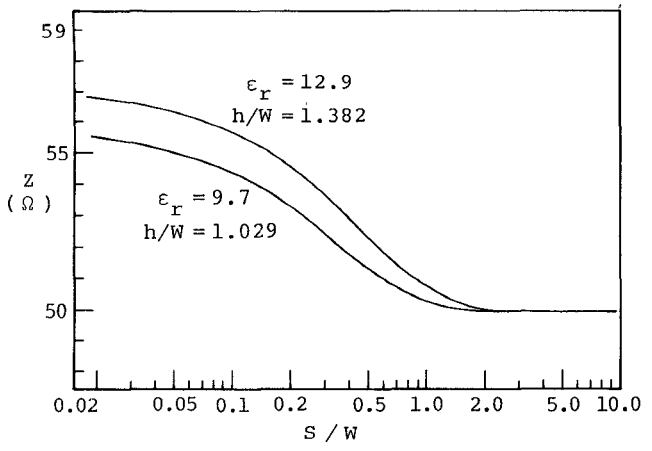

Fig. 6. Estimated proximity effects on the characteristic impedance.

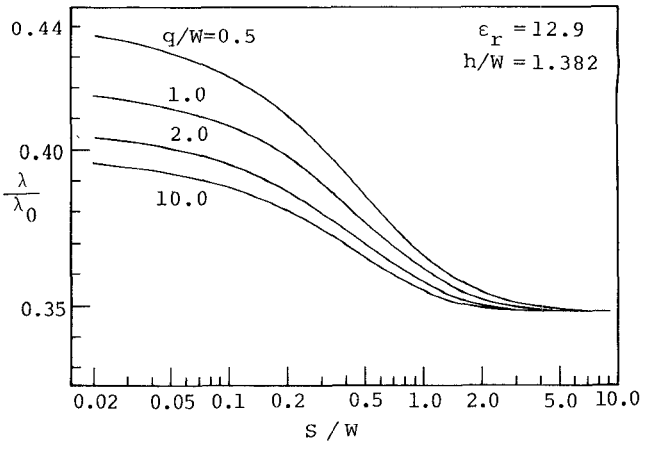

Fig. 9. Estimated proximity effects of conductor wall and substrate edge on the wavelength reduction factor.

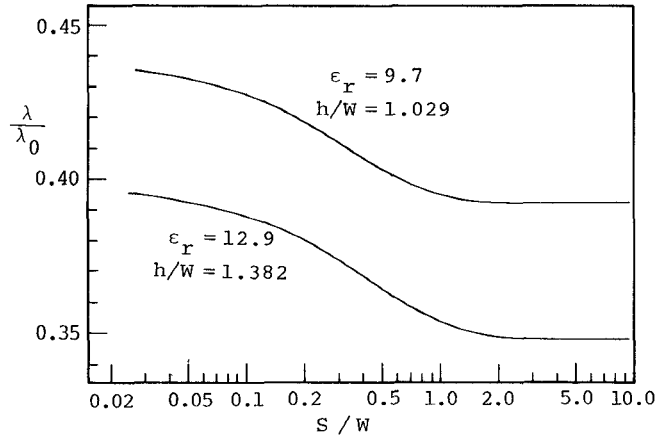

Fig. 7. Estimated proximity effects on the wavelength reduction factor.

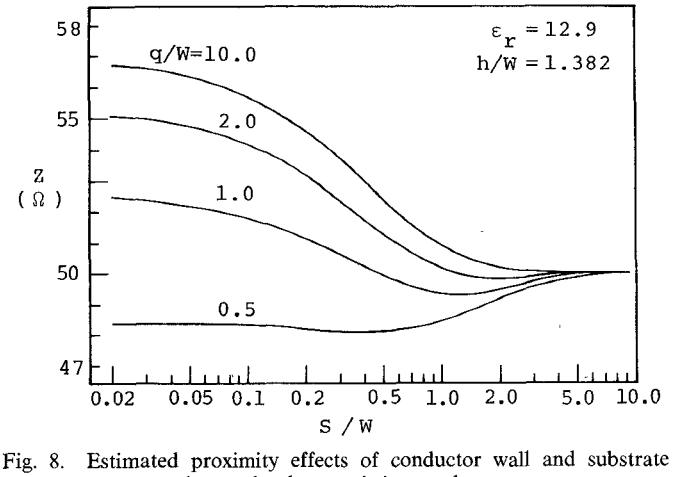

Fig. 8. Estimated proximity effects of conductor wall and substrate edge on the characteristic impedance.

The line capacitance (per unit length) was measured to confirm theoretical results on the proximity effects by using a Boonton 72-BD capacitance meter. Experimental parameters of our sample transmission line were $\epsilon_r = 2.55$ (polystyrene), $W = 4.02$ mm, and $h = 10.45$ mm. Measured capacitance values are compared with theoretical ones in Fig. 10. These results agree with our analysis with errors of about 1 percent.

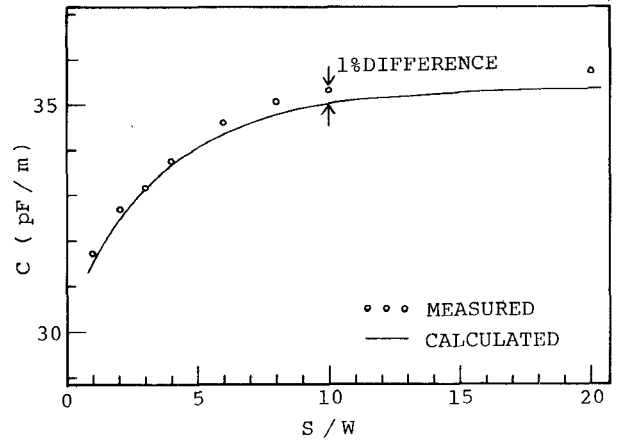

Fig. 10. Measured line capacitance values compared with theoretical values for sample line parameters, $\epsilon_r = 2.55$ (polystyrene), $W = 4.02$ mm, and $h = 10.45$ mm

IV. Edge-Compensated Microstrip Lines

As can be observed from the above results, all of the proximity effects on the transmission characteristics are caused by the fact that the electric field is no longer completely concentrated in the dielectric substrate but rather is partly located in the air, namely, by the decrease of the line capacitance.

A way to compensate for the proximity effects is to increase the line capacitance by widening the strip conductor width. Hence, we propose an edge-compensated microstrip line (ECM line), whose structure is as shown in Fig. 1.

The necessary dimensions of the strip width of ECM lines for keeping the characteristic impedance constant can be found by using the above analysis method. Fig. 11 shows the calculated strip width of 50 Ω ECM lines for the case of GaAs and alumina ceramic substrate, where W_0 is defined as the strip width of a classical 50 Ω microstrip line for the same substrate material. Fig. 12 shows the wavelength reduction factor for the 50 Ω ECM lines thus designed.

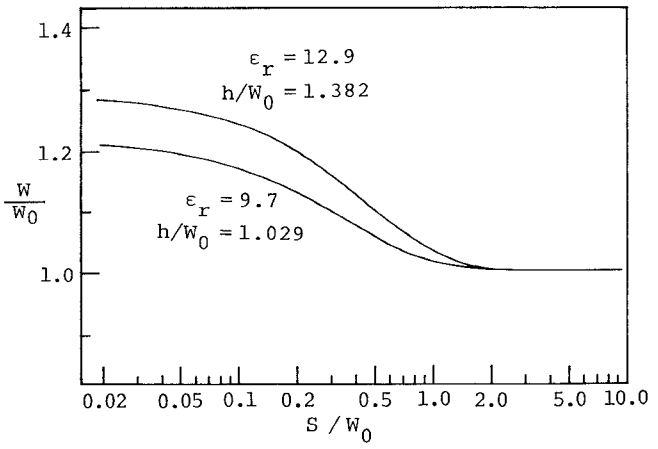

Fig. 11. Designed strip width of 50 Ω ECM lines.

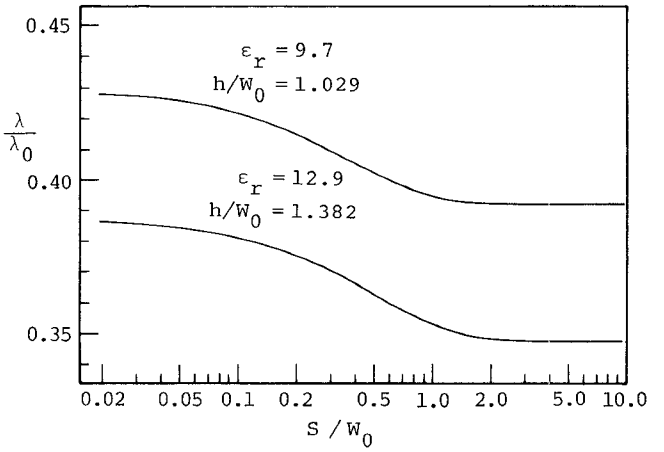

Fig. 12. Wavelength reduction factor of 50 Ω ECM lines.

V. Approximate Polynomial Formulas

The above numerical data on ECM lines can also be expressed in simple approximate formulas by a least-square curve-fitting procedure. The following polynomial formulas give the designed strip width W and the wavelength reduction factor λ/λ_0 of 50 Ω ECM lines in terms of the separation S normalized by the 50 Ω microstrip with W_0:

$$\frac{W}{W_0} = \sum_{n=0}^{6} a_n u^n \qquad (0.1 \leqslant S/W_0 \leqslant 5.0) \qquad (14)$$

$$\frac{\lambda}{\lambda_0} = \sum_{n=0}^{6} b_n u^n \qquad (0.1 \leqslant S/W_0 \leqslant 5.0) \qquad (15)$$

where $u = \log_{10}(S/W_0)$, and the coefficients of the polynomials, a_n and b_n, for GaAs and alumina ceramic substrate are given in Table I. The errors of these polynomial formulas against the above theoretical results are less than 1 percent.

TABLE I
Coefficients of the Polynomials in the Approximate Design Formulas of 50 Ω ECM Lines

POLYNOMIAL COEFFICIENTS				
	GaAs		Alumina Ceramic	
ε_r	12.9		9.7	
h/W_0	1.382		1.029	
i	a_i	b_i	a_i	b_i
0	1.0367	$3.5346\cdot10^{-1}$	1.0162	$3.9554\cdot10^{-1}$
1	$-1.8228\ 10^{-1}$	$-2.5010\cdot10^{-2}$	$-9.8654\cdot10^{-2}$	$-1.7792\cdot10^{-2}$
2	$1.7147\cdot10^{-1}$	$2.2373\cdot10^{-2}$	$1.3236\cdot10^{-1}$	$2.2627\cdot10^{-2}$
3	$1.3289\cdot10^{-1}$	$1.8016\cdot10^{-2}$	$3.3574\cdot10^{-2}$	$6.8338\cdot10^{-3}$
4	$-8.0565\ 10^{-2}$	$-1.0253\cdot10^{-2}$	$-7.0952\ 10^{-2}$	$-1.2018\cdot10^{-2}$
5	$-8.1078\cdot10^{-2}$	$-1.0717\cdot10^{-2}$	$-2.4336\cdot10^{-2}$	$-4.6957\cdot10^{-3}$
6	$-1.5946\cdot10^{-2}$	$-2.1593\cdot10^{-3}$	$2.2125\cdot10^{-3}$	$1.9738\cdot10^{-3}$

VI. Conclusion

In this paper, we described an analysis method for the proximity effects in high-packing-density MMIC's, the characteristics of proposed ECM lines as a measure of the proximity effects, and simple polynomial formulas for the design of 50 Ω ECM lines.

The numerical convergence of the transmission parameters with this method was satisfactory for reasonable numbers of Fourier terms and spline-knots. Although some approximations, such as a thin-strip conductor, have been made in this analysis, experimental results on the line capacitance have indicated good agreement with theory.

Appendix I

The symbols appearing in (5a), (5b), and (5c) are defined as follows:

$$A_{ni} = \begin{cases} \xi_{1n}^{-2}\left[\dfrac{\sin(\xi_{1n}x_i)-\sin(\xi_{1n}x_{i-1})}{x_i - x_{i-1}} - \dfrac{\sin(\xi_{1n}x_{i+1})-\sin(\xi_{1n}x_i)}{x_{i+1}-x_i}\right] & (i=1,2,\cdots,k-1) \\ \xi_{1n}^{-2}\dfrac{\sin(\xi_{1n}x_k)-\sin(\xi_{1n}x_{k-1})}{x_k - x_{k-1}} & (i=k) \end{cases} \qquad (A1)$$

$$B_{ni}=\begin{cases}\xi_{2n}^{-2}\left[\dfrac{\sin(\xi_{2n}x_i)-\sin(\xi_{2n}x_{i-1})}{x_i-x_{i-1}}-\dfrac{\sin(\xi_{2n}x_{i+1})-\sin(\xi_{2n}x_i)}{x_{i+1}-x_i}\right] & (i=k+1,k+2,\cdots,m-1)\\ -\xi_{2n}^{-2}\dfrac{\sin(\xi_{2n}x_{k+1})-\sin(\xi_{2n}x_k)}{x_{k+1}-x_k} & (i=k)\end{cases} \tag{A2}$$

$$C_{ni}=\xi_{3n}^{-2}\left[\frac{\sin(\xi_{3n}x_i)-\sin(\xi_{3n}x_{i-1})}{x_i-x_{i-1}}-\frac{\sin(\xi_{3n}x_{i+1})-\sin(\xi_{3n}x_i)}{x_{i+1}-x_i}\right] \qquad (i=1,2,\cdots,m-1). \tag{A3}$$

Appendix II

The symbols appearing in (6) are defined as follows:

$$\alpha_{ij}=\alpha_{1ij}+\alpha_{2ij}+\alpha_{3ij}+\alpha_{4ij} \tag{A4}$$

$$\alpha_{1ij}=\begin{cases}\displaystyle\sum_{n=1}^{\infty}\frac{\epsilon\xi_{1n}}{p\tanh(\xi_{1n}h)}A_{ni}A_{nj} & (i,j=1,2,\cdots,k)\\ 0 & (\text{otherwise})\end{cases} \tag{A5}$$

$$\alpha_{2ij}=\begin{cases}\displaystyle\sum_{n=1}^{\infty}\frac{\epsilon_0\xi_{2n}}{q\tanh(\xi_{2n}h)}B_{ni}B_{nj} & (i,j=k,k+1,\cdots,m-1)\\ 0 & (\text{otherwise})\end{cases} \tag{A6}$$

$$\alpha_{3ij}=\sum_{n=1}^{\infty}\frac{\epsilon_0\xi_{3n}}{a\tanh(\xi_{3n}(b-h))}C_{ni}C_{nj} \qquad (i,j=1,2,\cdots,m-1) \tag{A7}$$

$$\alpha_{4ij}=\begin{cases}-\displaystyle\sum_{n=1}^{\infty}\frac{(-1)^n}{n\pi h}\epsilon A_{ni} & (i=1,2,\cdots,k-1;\ j=k)\\ -\displaystyle\sum_{n=1}^{\infty}\frac{(-1)^n}{n\pi h}\epsilon A_{nj} & (i=k;\ j=1,2,\cdots,k-1)\\ -\displaystyle\sum_{n=1}^{\infty}\frac{(-1)^n}{n\pi h}\epsilon_0 B_{ni} & (i=k+1,\ k+2,\cdots,m-1;\ j=k)\\ -\displaystyle\sum_{n=1}^{\infty}\frac{(-1)^n}{n\pi h}\epsilon_0 B_{nj} & (i=k;\ j=k+1,\ k+2,\cdots,m-1)\\ \dfrac{\epsilon}{6}\left(\dfrac{h}{p}+\dfrac{p}{h}\right)+\dfrac{\epsilon_0}{6}\left(\dfrac{h}{q}+\dfrac{q}{h}\right)-2\displaystyle\sum_{n=1}^{\infty}\frac{(-1)^n}{n\pi h}(\epsilon A_{nk}+\epsilon_0 B_{nk}) & (i=j=k)\\ 0 & (\text{otherwise}).\end{cases} \tag{A8}$$

Acknowledgment

The authors thank Dr. N. Kishi for his helpful comments.

References

[1] R. A. Pucel, "Design consideration for monolithic microwave circuits," *IEEE Trans. Microwave Theory Tech.*, vol. MTT-29, pp. 513–534, June 1981.

[2] R. A. Pucel, "MMIC's modeling and CAD-Where do we go from here?" in *Proc. 16th European Microwave Conf.*, Sept. 1986, pp. 61–70.

[3] E. Yamashita, K. R. Li, and Y. Suzuki, "Characterization method and simple design formulas of MCS lines proposed for MMIC's," *IEEE Trans. Microwave Theory Tech.*, vol. MTT-35, pp 1355–1362, Dec. 1987.

[4] C. E. Smith and R. Chang, "Microstrip transmission line with finite-width dielectric," *IEEE Trans. Microwave Theory Tech.*, vol. MTT-28, pp. 90–94, Feb. 1980.

[5] E. Yamashita, M. Nakajima, and K. Atsuki, "Analysis method for generalized suspended striplines," *IEEE Trans. Microwave Theory Tech.*, vol. MTT-34, pp. 1457–1463, Dec. 1986.

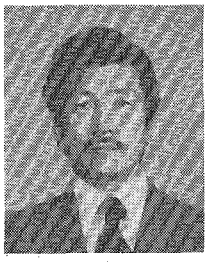

Eikichi Yamashita (M'66–SM'79–F'84) was born in Tokyo, Japan, on February 4, 1933. He received the B.S. degree from the University of Electro-communications, Tokyo, Japan, and the M.S. and Ph.D. degrees from the University of Illinois, Urbana, all in electrical engineering, in 1956, 1963, and 1966, respectively.

From 1956 to 1964, he was a member of the Research Staff on millimeter-wave engineering at the Electrotechnical Laboratory, Tokyo, Japan. While on leave from 1961 to 1963 and from 1964 to 1966, he studied solid-state devices in the millimeter-wave region at the Electro-Physics Laboratory, University of Illinois. From 1966 to 1967, he was with the Antenna Laboratory, University of Illinois. He became Associate Professor in 1967 and Professor in 1977 in the Department of Applied Electronics, the University of Electro-communications, Tokyo, Japan. His research work since 1956 has been on microstrip transmission lines, suspended striplines, wave propagation in gaseous plasma, pyroelectric-effect detectors in the submillimeter-wave region, tunnel-diode oscillators, wide-band laser modulators, and various types of optical fibers.

Dr. Yamashita is a member of the Institute of Electronics, Information and Communication Engineers of Japan and Sigma Xi. During the period 1980–1984, he served as Associate Editor of the IEEE TRANSACTIONS ON MICROWAVE THEORY AND TECHNIQUES. He was elected chairman of the Tokyo chapter of the MTT Society for the period 1985–1986.

✠

Hideyuki Ohashi was born in Kanagawa, Japan, on September 23, 1963. He received the B.S. and M.S. degrees in electrical engineering from the University of Electro-communications, Tokyo, Japan, in 1986 and 1988, respectively.

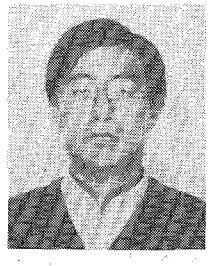

He is presently with the Information Systems and Electronics Development Laboratory, Mitsubishi Electric Corporation, Kamakura, Japan.

✠

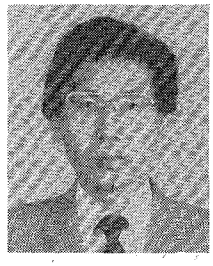

Kazuhiko Atsuki was born in Tokyo, Japan, on November 2, 1942. He received the B.S. and M.S. degrees from the University of Electro-communications, Tokyo, Japan, and the Dr. Eng. degree from the University of Tokyo, Tokyo, Japan, all in electrical engineering, in 1965, 1967, and 1979, respectively.

He became a Research Assistant in 1967, an Instructor in 1979, and in 1982 an Associate Professor in the Department of Applied Electronics, University of Electro-communications, Tokyo, Japan. His research has dealt with microstrip transmission lines, wide-band laser modulators, and optical fibers.

Dr. Atsuki is a member of the Institute of Electronics and Communication Engineers of Japan.